$$\Delta 2\theta = 360s\cos\theta/\pi R, \tag{3.3.13}$$

where R is the goniometer radius. This is the major peak-displacement effect and can be detected for sample displacements as small as 10 μm.

A similar effect can be observed for Debye–Scherrer instrumentation when the goniometer axis is not coincident with the sample axis; this is a more common problem for neutron powder diffraction instruments where accurate placement of very massive goniometers can be difficult. In this case the peak displacement is

$$\Delta 2\theta = \frac{180}{\pi R}(s_x\cos 2\theta + s_y\sin 2\theta), \tag{3.3.14}$$

where s_x and s_y are displacements perpendicular and parallel to the incident beam, respectively, all in the diffraction plane.

In high-resolution instrumentation (even at a synchrotron) goniometer axis displacements less than 10 μm can be detected.

Specimen transparency in Bragg–Brentano diffraction can also cause peak displacements arising from the shift in effective sample position to below the surface at high scattering angles. This shift for a thick specimen is

$$\Delta 2\theta = 90\sin 2\theta/\mu_{\rm eff}\pi R, \tag{3.3.15}$$

where $\mu_{\rm eff}$ is the effective sample absorption coefficient taking into account the packing density.

3.3.2.4. *Fundamental parameters profile modelling*

An alternative method for describing the source and instrumental part of the powder peak profile is to develop a set of individual functions that form the part of the profile arising from each of the instrumental components that shape the beam profile (Cheary & Coelho, 1992, 1998*a*,*b*). Ideally, each function is parameterized in terms of the physical parameters of the corresponding instrument component (*e.g.* slit width and height, sample dimensions and absorption, source size and emission characteristics, *etc.*), which are known from direct measurement. The set of functions are then convoluted *via* fast mathematical procedures to produce a line profile that matches the observed one. Any remaining profile-broadening parameters (*e.g.* for sample crystallite size and microstrain, see Section 3.3.5 for details) are then allowed to adjust during a Rietveld refinement. By employing this fundamental parameters (FP) approach, these parameters are unaffected by any instrumental parameterization.

The FP method offers two clear advantages over the more empirical approach outlined in Sections 3.3.2.1–3.3.2.3 above: (i) it can more closely describe the actual instrumental effects that contribute to the profile shape, thus improving the precision of the fit to the observed data and (ii) it can be used to describe a source characteristic or an instrumental arrangement that is outside the normally used configuration, yielding a result that would be difficult to obtain otherwise (Cheary *et al.*, 2004).

3.3.3. Peak profiles for neutron time-of-flight experiments

3.3.3.1. *The experiment*

The neutron source in a time-of-flight (TOF) powder diffraction experiment produces pulses of polychromatic neutrons; these travel over the distance from the source to the sample and then to the detectors which are placed at fixed scattering angles about the sample position; the travel times are of the order of 1–100 ms. This has been briefly described in Volume C of *International Tables for Crystallography* (Jorgensen *et al.*, 1992). Because neutrons of differing velocities (v) have differing wavelengths (λ) according to the de Broglie relationship ($\lambda = h/mv$) given Planck's constant (h) and the neutron mass (m), they will sort themselves out in their time of arrival at the detector. The powder pattern appears as a function of TOF *via* Bragg's law ($\lambda = 2d\sin\theta$) in which the wavelength is varied and θ is fixed. The approximate relationship between TOF, wavelength and d-spacing observed in a particular detector can be derived from the de Broglie relationship and Bragg's law to give

$$\text{TOF} = 252.7784L\lambda = 505.5568Ld\sin\theta. \tag{3.3.16}$$

The constants are such that given λ in ångströms and the total neutron flight path length L in metres, then the TOF will be in μs. An analysis of the possible variances in these components then gives an estimate of the powder diffraction peak widths:

$$\Delta d/d = [(\Delta t/t)^2 + (\Delta\theta\cot\theta)^2 + (\Delta L/L)^2]^{1/2}, \tag{3.3.17}$$

where Δd, Δt, $\Delta\theta$ and ΔL are, respectively, the uncertainties in d-spacing, TOF, scattering angle θ and total flight path L (Jorgensen & Rotella, 1982). Consequently, these three terms also determine the instrumental contribution to the neutron TOF powder peak profile.

3.3.3.2. *The neutron pulse shape*

The neutron pulse shape depends on the mode of production. Early studies (Buras & Holas, 1968; Turberfield, 1970) used one or more choppers to define a polychromatic pulse from a reactor source, resulting in essentially Gaussian powder peak profiles whose FWHM (Γ_G) is nearly constant ($B \simeq 0$):

$$\Gamma_G^2 = A + Bd^2, \tag{3.3.18}$$

so that the Rietveld technique can easily be used (*e.g.* Worlton *et al.*, 1976). Unfortunately, this approach gave very low intensities and relatively low resolution powder patterns.

A more useful approach uses a spallation source to produce the pulsed neutron beam. Neutrons are produced when a high-energy proton beam (>500 MeV) strikes a heavy metal target (usually W, U or liquid Hg) *via* a spallation process (Carpenter *et al.*, 1984). These very high energy neutrons strike small containers of moderating material (usually H_2O, liquid CH_4 or liquid H_2) which then comprise the neutron source seen by the powder diffraction instrument. The entire target/moderator system is encased in a neutron-reflective material (usually Be) to enhance the neutron flux and then further encased in a biological shield. Each moderator may be encased on the sides away from the instrument (*e.g.* powder diffractometer) in a thin neutron absorber (*e.g.* Cd or Gd) and may also contain an inner absorber layer ('poison') to sharpen the resulting pulse of thermal neutrons. These sources produce a polychromatic neutron beam that is rich in both thermal (<300 meV) and epithermal (>300 meV) neutrons. The proton pulses can have a very short duration (~200 ns) (from a 'short-pulse' source, *e.g.* ISIS, Rutherford Laboratory, UK or LANSCE, Los Alamos National Laboratory, USA) or a much longer duration (>500 ns) (a 'long-pulse' source, *e.g.* SNS, Oak Ridge National Laboratory, USA or ESS, European Spallation Source, Sweden); the pulse repetition rate at these sources is 10–60 Hz. These characteristics are largely dictated by the proton accelerator and neutron source design. The resulting neutron pulse results from complex down-scattering and thermalization processes in the whole target/moderator assembly; it may be further shaped by choppers,

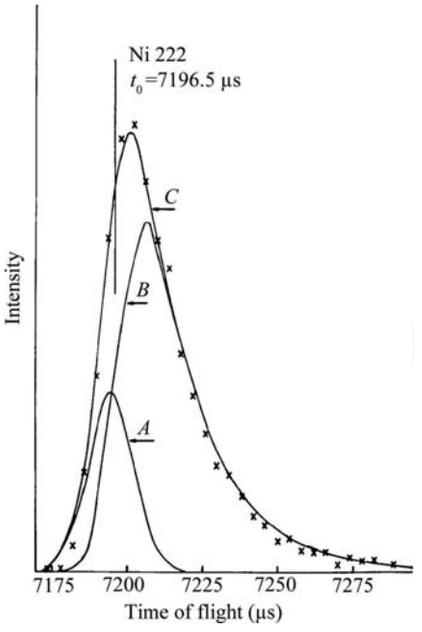

Figure 3.3.3
The observed and calculated Ni 222 diffraction line profile from the Back Scattering Spectrometer, Harwell Laboratory, Chilton, UK. The curves *A* and *B* are computed from the two terms in equation (3.3.19) and curve *C* is the sum (from Von Dreele *et al.*, 1982).

particularly for long-pulse sources, to give what is seen at the powder diffractometer.

Consequently, the neutron pulse structure from these sources has a complex and asymmetric shape, usually characterized by a very sharp rise and a slower decay, both of which are dependent on the neutron wavelength. The resulting powder diffraction peak profile (Fig. 3.3.3) is then the convolution [equation (3.3.2)] of this pulse shape (G_λ) with symmetric functions (G_I) arising from beamline components (*e.g.* slits and choppers) and the sample characteristics (G_S).

3.3.3.3. *The neutron TOF powder peak profile*

An early attempt at representing the TOF peak profile used a piecewise approach combining a leading-edge Gaussian, a peak-top Gaussian and an exponential decay for the tail (Cole & Windsor, 1980). Although single peaks could be fitted well with this function, the variation with TOF was complex and required many arbitrary coefficients.

A more successful approach empirically represented the pulse shape by a pair of back-to-back exponentials which were then convoluted with a Gaussian (Jorgensen *et al.*, 1978; Von Dreele *et al.*, 1982) to give

$$P(\Delta) = \frac{\alpha\beta}{\alpha+\beta}\left\{\exp\left[\frac{\alpha}{2}(\alpha\sigma^2+2\Delta)\right]\operatorname{erfc}\left[\frac{\alpha\sigma^2+\Delta}{\sigma(2^{1/2})}\right] + \exp\left[\frac{\beta}{2}(\beta\sigma^2-2\Delta)\right]\operatorname{erfc}\left[\frac{\beta\sigma^2-\Delta}{\sigma(2^{1/2})}\right]\right\}, \tag{3.3.19}$$

where α and β are, respectively, the coefficients for the exponential rise and decay functions; erfc is the complementary error function. Analysis of the data that were available then gave empirical relations for α, β and σ as

$$\alpha = \alpha_1/d; \quad \beta = \beta_0 + (\beta_1/d^4); \quad \sigma = \sigma_1 d. \tag{3.3.20}$$

The two terms in this function are shown in Fig. 3.3.3. The junction of the two exponentials defines the peak position (shown as a vertical line in Fig. 3.3.3); it is offset to the low side of the peak maximum. This arbitrary choice of peak position then affects the relationship between the TOF and reflection *d*-spacing; an empirical relationship (Von Dreele *et al.*, 1982) was found to suffice:

$$\mathrm{TOF} = Cd + Ad^2 + Z, \tag{3.3.21}$$

with three adjustable coefficients (C, A, Z) established *via* fitting to the pattern from a standard reference material.

Although this profile description was adequate for room-temperature moderators (H_2O or polyethylene) at low-power spallation sources, it does not describe well the wavelength dependence for cold moderators feeding neutron guides used at higher-power sources. An alternative description, employing a switch function to account for the fundamental change in the neutron leakage profile from the moderator between epithermal and thermal neutrons, was proposed (Ikeda & Carpenter, 1985; Robinson & Carpenter, 1990) to accommodate the profiles seen from liquid CH_4 or H_2 moderators. A drawback of this description is that the pulse profile is defined with the peak position at the low TOF edge; convolution with G_I and G_S results in a function where the peak position is far below the peak top. An empirical approach by Avdeev *et al.* (2007) simply requires tables to be established from individual peak fits to a standard material powder pattern for the values of α, β and TOF in place of the expressions given in equations (3.3.20) and (3.3.21); this establishes the G_λ and G_I contributions to the TOF line shape. More recently, some simple extensions (Toby & Von Dreele, 2013) to the empirical functions [equations (3.3.22) and (3.3.23)] appear to better cover the deviations arising from the enhanced epithermal contribution to the cold moderator spectrum:

$$\mathrm{TOF} = Cd + Ad^2 + B/d + Z, \tag{3.3.22}$$

$$\alpha = \frac{\alpha_1}{d}; \quad \beta = \beta_0 + \frac{\beta_1}{d^4} + \frac{\beta_2}{d^2}; \quad \sigma = \sigma_0 + \sigma_1 d^2 + \sigma_2 d^4 + \frac{\sigma_3}{d^2}. \tag{3.3.23}$$

3.3.4. Peak profiles for X-ray energy-dispersive experiments

In an X-ray dispersive powder diffraction experiment, a detector with good energy-discrimination capability is placed at a fixed scattering angle while the sample is illuminated by a 'white' beam of radiation. The detector response is binned into discrete energies by a multichannel analyser (MCA) (Glazer *et al.*, 1978). Typically these instruments display peaks that are purely Gaussian in shape with quite low resolution ($\Delta E/E \simeq 1\%$) and have widths that are proportional to the energy:

$$\Gamma_G = UE + W. \tag{3.3.24}$$

This is most useful for experiments with very limited angular access (*e.g.* high-pressure multi-anvil setups, as described in Chapter 2.7) using synchrotron radiation and can give very high data collection rates on very small samples. Glazer *et al.* (1978) showed that simple crystal structures can be modelled with the Rietveld technique after suitable corrections to account for the variation in source intensity, detector response and sample absorption effects. Otto (1997) expanded the peak-profile description to include possible sample-broadening effects *via* a Voigt profile; this extended the expression in equation (3.3.24) by adding a second-order term in energy and allowed extraction of